EUROPEAN FUSION DEVELOPMENT AGREEMENT

EFDA-JET-CP(05)02-29

F. Imbeaux, J.F. Artaud, J. Kinsey, T.J.J. Tala, C. Bourdelle, T. Fujita,
C. Greenfield, E. Joffrin, Y.S. Na, V.V. Parail, Y. Sakamoto, A.C.C. Sips,
I. Voitsekovitch and JET EFDA contributors

Multi-Machine Transport Analysis of Hybrid Discharges from the ITPA Profile Database

Multi-Machine Transport Analysis of Hybrid Discharges from the ITPA Profile Database

F. Imbeaux[1], J.F. Artaud[1], J. Kinsey[2], T.J.J. Tala[3], C. Bourdelle[1], T. Fujita[4], C. Greenfield[5], E. Joffrin[1], Y.S. Na[6,7], V.V. Parail[8], Y. Sakamoto[4], A.C.C. Sips[6], I. Voitsekovitch[8] and JET EFDA contributors*

[1]Association EURATOM-CEA, CEA/DSM/DRFC, CEA Cadarache, France
[2]Lehigh University, Bethlehem, PA 18015, USA
[3]Association EURATOM-Tekes, VTT Process, Finland
[4]Naka Fusion Research Establishment, Japan Atomic Energy Research Institute, Naka-machi, Naka-gun, Ibaraki-ken 311-0193, Japan
[5]General Atomics, San Diego, USA
[6]Max-Planck-Institut für Plasmaphysik, EURATOM-IPP Association, Garching, Germany
[7]Korea Basic Science Institute, 52 Yeoeun-Dong, Yusung-Gu, Daejeon, 305-333, Korea
** See annex of J. Pamela et al, "Overview of JET Results ", (Proc.20 [th] IAEA Fusion Energy Conference, Vilamoura, Portugal (2004).*

Preprint of Paper to be submitted for publication in Proceedings of the EPS Conference,
(Tarragona, Spain 27th June - 1st July 2005)

ABSTRACT:
Current diffusion, heat transport modelling, and linear gyrokinetic stability analysis have been carried out on a set of 7 hybrid discharges from AUG, DIII-D, JET and JT-60U, in order to gain better understanding of the physics underlying this promising candidate scenario for ITER. Within this dataset, the GLF23 model has a higher accuracy than the Weiland model in predicting the temperature profiles in the region $0.3 < \beta < 0.8$. The core heat transport appears to be similar between hybrid discharges and standard H-modes, and also among hybrid discharges with very different H factors. Projections to ITER show that $Q = 10$ can be obtained with the hybrid scenario using an alternative scaling without β degradation. However, additional off-axis current drive and current profile control might be needed for the ITER hybrid scenario, in order to achieve its full potential for high β_N on extended duration.

1. INTRODUCTION

The reference target performance for the experimental fusion reactor ITER is to achieve a stationary fusion gain Q of the order of 10, where Q is the ratio of the power provided by fusion reactions to the auxiliary power needed to heat the plasma [1]. In the temperature range expected for a fusion reactor (10-20keV), the fusion gain increases faster than linearly with the triple product $nT\tau_E = \left(nT\tau_E \propto \frac{Q}{Q+5} \right)$, those three quantities being respectively the density, the ion temperature, and the energy confinement time [2]. In order to achieve $Q = 10$, the ITER reference scenario operates at high plasma current (I_p = 15MA, safety factor at 95% of the toroidal flux q_{95} = 3), taking advantage of the almost proportional dependence of the energy confinement time on I_p. Indeed the multi-machine empirical scaling expression used to extrapolate the energy confinement to ITER is [3]:

$$\tau_{E,th,IPB98(y,2)} = 0.0562 I^{0.93} B^{0.15} P^{-0.69} n^{0.41} M^{0.19} R^{1.97} \varepsilon^{0.58} \kappa_a^{0.78} \quad (1)$$

While operation at high I_p optimises the energy confinement time, it induces a limitation on the duration of the plasma discharge (about 400s at 15MA), owing to the small non-inductive current fraction. Moreover, the safety factor profile q is monotonic and tends to diffuse well below unity, which sets a limit to the pressure $P = nT$ that can be achieved without triggering deleterious Neoclassical Tearing Modes (NTM). This pressure limit is usually expressed in terms of the normalised ratio of the kinetic pressure to the magnetic pressure:

$$B_N = \frac{\frac{1}{V}\int P dV}{\frac{B^2}{2\mu_0}} \frac{100aB}{I_p} \quad (2)$$

where V is the plasma volume,B the toroidal magnetic field in Tesla, and$a$ the minor radius of the plasma in metres (I_p in MA). The ITER reference scenario operates at moderate β_N value 1.8, as a consequence of the reference H-mode scaling (1). This value is compatible with a broad q = 1 surface. However, operation at β_N value well above 2, that could be obtained with more additional heating or more favourable τ_E scaling are not compatible with the broad q = 1 surface that is characteristic of high current operation.

In the past years, alternative "advanced" scenarios have been proposed to extend the duration of the discharge in ITER, and even achieve fully steady-state operation [4]. The present work focuses on the so-called "hybrid" scenario, which might achieve the same fusion gain as the reference scenario Q = 10 with a increased discharge duration and plasma pressure. The hybrid scenario operates at a slightly lower current than the reference scenario, which allows to increase the plasma duration, owing to a reduction of the transformer flux consumption during both the current ramp-up and flat-top. In order to compensate the decrease of Q due to the reduced I_P value, the pressure has to be increased. This should also be allowed by the lower I_P : pushing the central safety factor q_0 towards 1 or even above 1 with a flatter q-profile in the plasma core increases the stability to deleterious NTM. Operation with $\beta_N \sim 3$, close to the no-wall limit, is foreseen. Thus the hybrid scenario is a promising concept for achieving Q = 10 with increased plasma duration and neutron fluence.

"Hybrid" H-mode discharges at moderate current (q_{95} = 3.2 – 4.5) and high β_N (up to ~ 3.5) have now been obtained in various tokamaks, for instance : ASDEX-Upgrade (AUG) [5], DIII-D [6], JET [7], JT-60U [8]. Operation without sawteeth in the plasma ($q > 1$ everywhere) allows to operate close to the no-wall β_N limit. This is usually achieved by reducing the plasma current, i.e. $q_{95} \leq 4$. Note that DIII-D has also developed a hybrid scenario at lower $q_{95} \approx 3.2$, with sawteeth and ELMs that are small enough to avoid the triggering of deleterious NTMs below β_N = 2.8 [6]. Though this limit is lower than in the case without any sawteeth $q_{95} \leq 4$, it remains higher than for the standard Elmy-H mode. These experimental results reflect the key concepts of the hybrid scenario: to reduce the background MHD activity by tailoring the q-profile, so that high β_N can be achieved without triggering deleterious NTM.

In addition to the high β_N performances, hybrid discharges have also achieved improved energy confinement with respect to the IPB98 scaling expression (1). The H factor, defined as the ratio of the experimental energy confinement time to the one predicted by the scaling ($= \tau_{E,exp}/\tau_{E,scaling}$) can reach values ranging between 1 and 1.6. The reasons for these high values of the H factor are not fully understood yet, nor the origin of its large scatter among the hybrid discharges of the various tokamaks. Moreover, the physics of the dynamics of the q-profile in the hybrid discharges is not completely clarified either. Therefore there is an important motivation to carry out detailed modelling of these discharges, in order to gain better understanding of the physics and also to define a modelling strategy to extrapolate this regime to ITER. These are the aims of the present work.

In the framework of the ITPA group on Transport Physics and the ITB Database working group, profile data for a set of seven hybrid discharges from various tokamaks has been collected (Asdex

Upgrade (AUG), DIII-D, JET, and JT-60U). The dataset is presented in section 2. In this work, various kinds of analysis are carried out on this dataset : simulation of current diffusion (section 2), linear turbulence stability analysis (section 3), and heat transport modelling (section 4). In section 5, some issues about the extrapolation of the hybrid regime to ITER are discussed, and illustrated by some examples of integrated modelling.

2. PRESENTATION OF THE DATASET

Table 1 summarises the main characteristics of the selected hybrid discharges, which feature a significant variation in density. The discharges are mainly heated by Neutral Beam Injection (NBI), with in some cases a small amount of Ion or Electron Cyclotron Resonance Heating (ICRH or ECRH). All discharges are based on the same scenario : strong NBI heating is applied during or just after the current ramp-up, with the appropriate timing so that the $q = 1$ surface does not appear in the plasma core. The JT-60U discharge is slightly different from the others since it features an Internal Transport Barrier (ITB) near $r = 0.4$ (r being the toroidal flux coordinate). It is a high β_p Elmy H-mode that features a flat central q profile above 1, where $\beta_N = 2.5$ has been sustained for 15.5s [9].

The profile data gathered for this study is not time-dependent. The analysis focuses on one time slice per shot, which corresponds to a stationary high performance phase.

3. Q-PROFILE MODELLING

Current diffusion simulations have been carried out using the CRONOS integrated modelling code [10]. Density and temperatures are prescribed and taken from the experiment. The NBI current drive (and EC current drive for the JT-60U shot) is also taken as an input, being calculated independently by each data provider. The bootstrap current is calculated inside CRONOS by the NCLASS module [11]. Since the experimental data correspond to a single stationary time slice per discharge, the simulation calculates the stationary solution of the current diffusion taking into account the various non-inductive current sources. The main purpose of these simulations is to test whether additional mechanisms have to be included in the simulation in order to obtain q-profiles without a significant $q = 1$ surface ($q > 1$ or $\rho_{q=1} < 0.1$). The absence of sawteeth in the discharges considered here is indeed an experimental evidence for $q > 1$, and also a key element to achieve high β_N in hybrid discharges.

The results of the simulations are contrasted depending on the discharge considered : no significant $q = 1$ surface is found for discharges JET60927, JET60931, DIIIID118348, and AUG16779, in agreement with the absence of sawteeth in the experiment at the time slice considered. However, a rather broad stationary $q = 1$ surface is found ($\rho_{q=1} > 0.2$) for the other discharges, i.e. DIIID118446, AUG17870, JT60U43903. Two examples are shown in Fig.1. Possible reasons for this discrepancy are i) uncertainties on the computed resistivity, ii) uncertainties on the calculated non-inductive sources (bootstrap, neutral beam driven current) and iii) additional effects, like the impact of benign NTM activity on the current diffusion. In particular, the exact amount of bootstrap current in the

pedestal is difficult to estimate since detailed measurements of the edge kinetic profiles are often not provided in the ITPA Profile database. The ongoing efforts to merge a detailed pedestal description (profiles and equilibrium) to the ITPA Profile database will allow a more detailed calculation.

The current density profile and current drive from the various non-inductive sources are shown in Fig.2. for the highest density shot of the dataset. The total non-inductive current fraction is about 60%, which is typical of hybrid shots with $q_{95} \sim 4$. Owing to the high density, the bootstrap current represents about 45% of the total plasma current. Both NBI and bootstrap current densities have broad profiles, therefore they tend to flatten the q-profile in the plasma core and push q_0 towards 1. Note that the pressure gradient at the pedestal drives a significant bootstrap current, between 10 – 20 % of the total current in typical hybrid discharges with $q_{95} \sim 4$.

Recent experiments on DIII-D have shown evidence of the effect of the mild NTM activity on the current profile in the hybrid regime [6]. Stabilisation of the $m = 3$, $n = 2$ NTM by localised co-ECCD provides a small decrease of the core q-profile and leads to the apparition of small sawteeth. Hence the (3,2) NTM helps to sustain q_0 above 1, however the amplitude of the effect appears to be rather small : the measured change of q_0 is found to be of the order of 0.05. Therefore a high fraction of off-axis non-inductive current (at least 50 - 60%) remains a necessary condition for sustaining a stationary q-profile with $q_0 \sim 1$.

4. LINEAR STABILITY ANALYSIS

The linear growth rates of turbulence eigenmodes have been calculated using two gyrokinetic codes, namely the GKS [12,13] and KINEZERO [14] codes. Such codes usually predict that turbulence modes are stable in the plasma core for $\rho < 0.2$-0.3. The situation is different for the hybrid shots of the present dataset, according to KINEZERO calculations that have been carried out for shots AUG 16779, JET 60931, DIIID 118348 and 118446, JT60U 43903. Indeed, all shots of this list but the JT-60U one are found linearly stable inside $\rho = 0.7$ for ITG, TEM, and ETGs. This is in contradiction with the heat diffusivities deduced from the experiment, which are well above the neoclassical values outside $\rho = 0.2$. In the JT-60U case, the temperature gradients are high enough around the ITB to have positive growth rates of ITGs (Fig.3). A stabilising mechanism is therefore needed to account for the ITB, likely ExB shearing. However, since the purpose of the present work is not to study ITBs, the detailed justification of the presence of this ITB is beyond the scope of this paper. The main point here is that in all hybrid shots without ITB analysed by KINEZERO, turbulent modes are found linearly stable from the centre to $\rho = 0.7$, in contradiction with the experimental heat diffusivities.

This analysis is confirmed by GKS runs carried out for the two DIII-D discharges. The plasma core is found stable to turbulence modes inside $\rho = 0.6$ (Fig.4). The ion diffusivity for these shots is 3 times (resp. 5 times) above the neoclassical value computed by NCLASS. Moreover, the gyrokinetic a/L_T threshold (where a is the minor radius and L_T the temperature gradient length, $1/\mathrm{lT}=\nabla T/T$) are at least a factor 2 above the experimental value (Fig.5). This suggests that the disagreement between

the linear gyrokinetic predictions and the experiment is outside the errobars on the determination of the experimental gradients (for such smooth temperature profiles).

Therefore, additional physics effects have to be taken into account in order to reconcile the theory predictions and the experiments. A likely candidate is non-local transport, i.e. the possibility that turbulence spreads from linearly unstable regions of the plasma (in its outer part) to linearly stable regions (inner part). This effect has been observed in global non-linear turbulence simulations [15]. Therefore these hybrid discharges are excellent test cases for benchmarking these non-local transport theories.

5. TEST OF FIRST-PRINCIPLE TRANSPORT MODELS

In this part, predictive heat transport simulations are carried out in order to test the predictive capability of two widely used first-principle transport models : the Weiland [16] and the GLF23 [17] models. The ion (T_i) and electron (T_e) temperatures are predicted while prescribing the density, toroidal rotation, and q-profile to their experimental values. The GLF23 simulations have been carried out using the CRONOS integrated modelling code, while the Weiland model simulations have been carried out using the JETTO code [18]. In the simulations, the boundary conditions and edge transport coefficients are set in order to match the experimental temperatures at ρ = 0.8. Therefore the profiles shown outside ρ = 0.8 do not correspond to the model predictions.

Figures 6 to 13 show the results obtained with the two models on the shots of the dataset. None of the models features a perfect agreement with the experimental profiles. GLF23 provides in general a correct stiffness ratio T(ρ = 0.3)/T (ρ = 0.8) especially for the DIII-D shots, the T_i of JET shots and the T_e of ASDEX shots (see Table 2). Note that this statement applies to the present dataset, and cannot be generalised to all hybrid shots from these tokamaks. GLF23 fails to reproduce the ITB structure of the JT-60U shot. The most important disagreement of the GLF23 model is found inside ρ = 0.3, where it predicts sometimes full turbulence stabilisation in contrast to the experiment (e.g. the strong temperature peaking of the DIII-D shots). The Weiland model can also produce accurate stiffness ratios, though often not on both channels (electron and ion) simultaneously. In contrast to GLF23, it predicts the temperature profiles of shot JT-60U 43903 rather accurately. It is difficult to draw general conclusions from the present analysis, since the accuracy of the models can differ a lot from one shot to the other, without a clear parametric trend. However, GLF23 shows a higher reliability than the Weiland model in predicting the average stiffness ratio T(ρ = 0.3)/T (ρ = 0.8), since it gives for this parameter a value within 20 % of the experimental one on 5 shots over 7 for both channels in the present dataset.

Note that in spite of the disagreement between gyrokinetic linear growth rate calculations and the experimental diffusivities (section 4), the two models tested here predict anomalous transport in the region 0.3 < ρ < 0.8. This could be expected from the Weiland model, which is based on a fluid theory and therefore should have lower thresholds than the gyrokinetic expressions. This is more surprising for the GLF23 model, that is based on a fit to the GKS linear growth rates [19]. It

appears that for the present dataset, GLF23's fit of GKS results is approximate, but eventually better fits the experiment. A rigorous way of improving fast first-principle models like GLF23 and Weiland could be to include non-local transport, on the basis of global non-linear simulations.

Another interesting point is that the accuracy of the first-principle models to reproduce the temperature profiles inside ρ = 0.8 does not depend on the *H* factor with respect to the IPB98 scaling expression (1). From the present modelling, there is no evidence that the core energy confinement is improved in correlation with the *H* factor. For instance, it has been shown in previous studies that GLF23 predicts a partial turbulence stabilisation by the ExB shearing rate [20]. However, the amplitude of the effect is among the present dataset not correlated to the *H* factor variation. Note that this partial turbulence stabilisation is also predicted for standard H mode discharges by GLF23, and hence is not specific to hybrid regimes [20]. Thus the physics-based models do not identify a clear reason why the core transport in hybrid regimes should be different from the standard H modes. This is consistent with previous AUG results showing that the T_i profile stiffness is the same between hybrid regimes and standard Elmy-H modes [21]. Some difference could still happen at the edge, which is beyond the scope of the present analysis. Recent results from AUG suggest that the pedestal of some hybrid discharges features a significant improvement with respect to the standard scaling expression for the pedestal pressure [22]. This has however to be confirmed on a broader database of hybrid discharges.

6. EXTRAPOLATION TO ITER

In this section, we show some examples of projections of the hybrid scenario to ITER using integrated modelling (CRONOS code). The purpose of this section is not to establish the definitive operation space of the hybrid scenarios to ITER, but rather to discuss some issues that are important for the extrapolation, based on a few simulations.

The most critical point for the extrapolation to ITER is the choice of the energy confinement model. We use here either a one-dimensional (1D) model where the diffusion coefficients are renormalised at each time step so that the confinement follows a global scaling law, either the GLF23 model. Another important point is the issue of predicting the pedestal height. In the case of the scaling-based model, two-terms scalings are used, i.e. the model makes the temperatures follow both a global scaling (core + pedestal energy content) and a separate scaling for either the core or the pedestal. Two sets of scaling are used here :

- Set A : global scaling IPB98 [3], core scaling ITER96-L (L mode scaling) [23]

$$\tau_{E,th,IPB98(y,2)} = 0.0562 I^{0.93} B^{0.15} P^{-0.69} n^{0.41} M^{0.19} R^{1.97} \varepsilon^{0.58} \kappa_a^{0.7}$$

$$\tau_{E,th,96-L} = 0.023 I^{0.96} B^{0.03} P^{-0.73} n^{0.40} M^{0.20} R^{1.83} \varepsilon^{-0.06} \kappa_a^{0.64}$$

- Set B : global scaling DS03 [24], combined to a pedestal scaling [25] :

$$\tau_{E,th,DS03} = 0.028 I^{0.83} B^{0.07} P^{-0.55} n^{0.49} M^{0.14} R^{1.81} a^{0.3} \kappa_a^{0.75}$$

$$\tau_{Eped,th} = 0.0209 I^{1.6} P^{-0.4} n^{-0.16} M^{0.20} R^{1.03} \varepsilon^{-0.26}$$

The set of scalings A assumes that the core of an H mode discharge has the same energy confinement as an L mode shot. In fact, the ITER reference scenario (standard H mode [1]) is compatible with this scaling if the resulting pedestal energy is reduced by a factor of 2. Therefore we present both a projection to the hybrid scenario i) with the set A as such, and ii) with a reduced pedestal energy so that $\tau_{E,ped,th} = \frac{\tau_{E,th,IPB98(y,2)} - \tau_{E,th,96-L}}{2}$ and $\tau_{E,core,th} = \frac{\tau_{E,th,IPB98(y,2)} + \tau_{E,th,96-L}}{2}$ which is conservative with respect to the standard H mode ITER reference scenario. The DS03 scaling has been proposed in [24] as an alternative scaling for H modes discharges with pure gyro-Bohm scaling and no β degradation. It is a more favourable scaling than IPB98 for the hybrid scenario, which aims at high β_N operation.

In the present extrapolations, we have chosen to use the global scaling expressions as such, i.e. with improvement factor $H = 1$. The main reason for this choice is to be conservative with respect to JET hybrid data, which feature $H_{98} < 1.2$ and $H_{DS03} \sim 1$ [7], while being the closest device to ITER in terms of size and ρ^* parameter.

In addition to the projections using this scaling law normalised model, we make use also of the GLF23 model. The model is however applied only between $0.3 < \rho < 0.8$. Indeed, inside $\rho = 0.3$, the model has been shown to predict sometimes too strong temperature peaking with respect to the experiment (section 5). An ad-hoc constant diffusion coefficient replaces the GLF23 model inside $\rho = 0.3$ in order to avoid such a strong temperature peaking. Moreover, as in section 5, GLF23 is used with the boundary condition at $\rho = 0.8$. We present here an example using the boundary condition provided by the favourable scaling set B.

The density profile is prescribed in these projections. We assume a strong density peaking so that $n_{e0} = 1.5\ n_{e,ped}$, which is compatible with the projections presented in [26]. The Greenwald fraction is 92 %, and $Z_{eff} = 1.8$ with a flat profile.

The plasma current is slightly reduced to 13 MA (against 15MA for the standard H-mode) in order not to lose too much on the energy confinement. Table 3 and Figure 14 summarise the main results of this projections. The DS03 scaling allows to reach the target
$Q = 10$ and even higher with a peaked density profile. The IPB98 scaling, as expected, provides much smaller Q values, of the order of 5. The GLF23 model gives a T_i profile very close to the DS03 projection. However, it should be stressed that the GLF23 model is quite stiff, therefore its prediction is strongly linked to the edge boundary condition. A more exhaustive study is needed to show the range of GLF23 predictions as a function of the pedestal height.

While, when using stiff first-principle models, the predicted core temperature increases strongly with the temperature at the top of the pedestal, the opposite behaviour is obtained with the 2-term scaling approach. Indeed, the global energy content is fixed by the global scaling expression, and distributed between the core and the pedestal. Therefore when the pedestal height is decreased, the lost energy content is given to the core. This is why the T_i profile becomes more peaked when the pedestal energy content is divided by 2 in the set of scalings A (bottom 2 lines of Table 3, and corresponding profiles on Fig.14).

As shown in Table 3, high β_N values are obtained with the DS03 scaling at I_p = 13MA, as expected in a hybrid scenario. As in present experiments, the q = 1 surface has to be avoided (or at least it should be kept narrow enough) in order to sustain high β_N without triggering deleterious NTM. Simulations of the current diffusion in ITER for various values of the plasma current show that, even if the occurrence of the q = 1 surface is delayed by the high electron temperature in the hybrid regime, it finally appears around 500-650s of discharge (Table 4). This might jeopardize the sustainment of high β_N on extended duration, which is the essence of the hybrid scenario for ITER. Therefore off-axis current drive can be important for the hybrid scenario, in order to control the penetration of the q = 1 surface. As shown in Table 4 and Fig.15, it is possible to delay by a factor of 1.6 the occurrence of the q = 1 surface and to reduce its size if a significant amount of off-axis current drive is added to the discharge. Figure 15 shows the delay in q-profile penetration obtained using 20 MW of Lower Hybrid Current Drive (LHCD). The LHCD is calculated here using the DELPHINE code [27], integrated to the CRONOS suite. The predicted current drive efficiency is about 2.5 10^{19} $AW^{-1}m^{-2}$ for a directivity of 70%, in line with previous predictions for the ITER steady-state scenario [28]. The LHCD increases and broadens the non-inductive current drive in two ways : i) it drives about 1 MA of off-axis current at ρ = 0.8 ii) it increases the global energy content, which increases the bootstrap current also by about 1MA.

It should be kept in mind that the current diffusion results above are strongly dependent on the assumptions on the energy confinement, because the bootstrap current is the dominant non-inductive current source in the ITER hybrid regime. In particular, the edge bootstrap current due to the pedestal pressure gradient represents a significant source of off-axis non-inductive current (11% to 25% of the total current in the simulations, see Table 4). Moreover, the possible influence of benign MHD on the current diffusion, as shown by DIII-D (see section 3) has been ignored in the simulations. However, it is quite difficult to predict what will be the amplitude of this effect in the hybrid scenario for ITER. Also the scenario may still be viable even if a small q = 1 surface is in the plasma, as for the low q_{95} DIII-D hybrid discharges. MHD models should be developed in order to predict what would be the β_N limit as a function of the size of the q = 1 surface. Again, these few simulations do not intend to be the definitive ITER projections of the hybrid scenario. Nevertheless, they show that current profile control might be needed also for the hybrid scenario, in order to fully achieve its potential for high β_N on extended duration.

CONCLUSIONS

Hybrid discharges are H modes with extended duration (lower Ip) and higher pressure (β_N). Owing to a large fraction of off-axis non-inductive current (at least 50-60%), their safety factor is of the order of 1 in the plasma core. Benign NTM activity like a small 3/2 NTM helps also to sustain $q_0 >$ 1 in discharges with $q_{95} \leq 4$, by increasing q_0 of the order of 0.05. However, a high fraction of off-axis non-inductive current remains a necessary condition to access to the hybrid regime. This specific q-profile provides a higher stability to deleterious NTM than in the standard Elmy H mode, which allows to achieve high β_N values.

Current diffusion, heat transport modelling, and linear gyrokinetic stability analysis have been carried out on a set of 7 hybrid discharges from AUG, DIII-D, JET and JT-60U. A first surprising result was that most of these discharges are found linearly stable in a very large core $\rho < 0.6$, while transport is clearly anomalous outside $\rho = 0.2$ for the discharges that have been analysed. Therefore these shots are excellent test cases for the most advanced gyrokinetic theories and codes, i.e. global non-linear calculations that may provide turbulence spreading and non-local transport. The GLF23 and Weiland model have been tested against the dataset. No systematic agreement is found, and the predictions can be in some cases quite far from the experiment. However, the GLF23 model presents the highest reliability in the prediction of the stiffness ratio $T(\rho = 0.3)/T(\rho = 0.8)$. Adding non-local features in such first-principle 1D models might help in increasing their accuracy in reproducing experimental data.

The main open issue for the understanding of the present hybrid discharges is related to the large scatter of improvement factor with respect to the various scaling expressions (both IPB98 and DS03). From the present modelling, there is no evidence that the core energy confinement is improved in correlation with the experimental H factor. It could mean that there is a real change in the edge physics that causes an improvement of the pedestal height. It is in any case an evidence that the existing scaling expressions are not relevant for this kind of discharges. Because of the more recent discovery of hybrid modes, the available scalings have been done on databases dominated by standard Elmy-H modes. Future work should try to reconcile standard Elmy-H modes and hybrid shots in a single global scaling, by building a database where they are equally weighted. Meanwhile, a careful and conservative approach to the extrapolation of the hybrid regime to ITER would be to use the existing scalings with H factor close to 1. Another approach is to use first-principle models, that reproduce the experimental data with similar accuracy whatever the H factor value. The main limitation of these models is that they can be used essentially for core transport, and need an additional model for predicting the pedestal height. Since these models are usually stiff, the predicted performances of the scenario essentially depend on the boundary condition. Using the DS03 scaling, the target $Q = 10$ could be reached at a reduced plasma current in ITER $I_P = 13$MA. However, even at reduced plasma current and high electron temperature, the $q = 1$ surface enters the plasma after about 650 s. Therefore current profile control might be needed also for the hybrid scenario, in order to achieve its potential for high β_N on extended duration.

ACKNOWLEDGEMENTS

The first author would like to acknowledge Dr. R. Waltz for fruitful scientific discussions on gyrokinetic simulations.

REFERENCES

[1]. Summary of the ITER Final Design Report 2001 ITER EDA Documentation Series No 22 (Vienna: IAEA)

[2]. Wesson J 1997 Tokamaks 2nd edition (Oxford: Clarendon Press)

[3]. ITER Physics Basis 1999 Nucl. Fusion **39** 2137

[4]. Sips ACC et al 2005 Plasma Phys. Control. Fusion **47** A19–A40

[5]. Staebler A et al., Proc. EX/4-5, IAEA Fusion Energy Conference 2004, Vilamoura, Portugal.

[6]. Wade M et al 2005 Nucl. Fusion **45** 407

[7]. Joffrin E et al., Proc. EX/4-2, IAEA Fusion Energy Conference 2004, Vilamoura, Portugal.

[8]. Suzuki T et al., Proc. EX/1-3, IAEA Fusion Energy Conference 2004, Vilamoura, Portugal.

[9]. Isayama A et al. 2005, Phys. Plasmas **12** 056117

[10]. Basiuk V et al. 2003, Nuclear Fusion **43** 822

[11]. Houlberg WA et al. 1997, Phys. Plasma **4** 3230

[12]. Kotschenreuther M et al. 1995, Comput. Phys. Commun. **88** 128

[13]. Waltz RE and Miller 1999 RL, Phys. Plasmas **6** 4264

[14]. Bourdelle C et al. 2002, Nuclear Fusion **42** 892

[15]. Waltz RE, Candy JM, and Rosenbluth MN 2002, Phys. Plasmas **9** 1938

[16]. Strand P et al. 1998 Nucl. Fusion **38** 545

[17]. Kinsey JE, Stabler GM and Waltz RE 2005, Phys. Plasmas 12 052503

[18]. Genacchi G and Taroni A 1988, report ENEA RT/TIB 1988(5)

[19]. Waltz RE et al. 1997, Phys. Plasmas **4** 2482

[20]. Kinsey JE et al. 2005 Nucl. Fusion **45** 1

[21]. Peeters A et al. 2002 Nucl. Fusion **42** 1376

[22]. Na YS et al., submitted to Nuclear Fusion

[23]. Kaye S et al. 1997, Nucl. Fusion **37** 1303

[24]. Petty C et al. 2003, Fus. Science tech. **43** 1

[25]. Cordey JG, private communication

[26]. Weisen H et al., Proc. EX/P6-31, IAEA Fusion Energy Conference 2004, Vilamoura, Portugal.

[27]. Imbeaux F 1999, report EUR-CEA-FC-1679

[28]. Houlberg W et al., submitted to Nucl. Fusion 2005

	Ip (MA)	Bt (T)	q_{95}	$\bar{n}$ (m^{-3})	T_{i0}/T_{e0}	ρ^* (10^{-3})	Heating	$n_{e0}/n_e^{(\rho = 0.8)}$	$\bar{n}/n_{GR}$
AUG 16779	1.0	2.4	4.3	4.3	1.9	5.1	NBI + ECRH	1.7	0.34
AUG 17870	1.0	2.1	3.7	5.0	1.3	6.1	NBI	1.8	0.39
DIII-D 118446	1.2	1.6	4.5	3.6	2.2	7.1	NBI	2.6	0.34
DIII-D 118348	1.2	1.6	4.5	6.9	1.2	6.0	NBI	1.3	0.65
JT-60U E43903	0.9	1.7	3.5	1.8	1.7	4.3	NBI + ECCD	2.2	0.45
JET 60927	1.4	1.7	4.2	3.4	1.5	4.4	NBI + ICRH	1.2	0.61
JET 60931	1.4	1.7	4.4	3.2	1.1	4.1	NBI + ICRH	1.1	0.58

JG05.339-1c

Table 1 : Main characteristics of the dataset used in the analysis.

	AUG 16779	AUG 17870	DIII-D 118446	DIII-D 118348	JT-60U 43903	JET 60927	JET 60931
$\bar{n}/n_{Gr}$	0.34	0.39	0.34	0.65	0.45	0.61	0.58
H_{98}	1.2	1.3	1.5	1.3	0.85	1.15	1.05
GLF28 $\Delta T_i@\rho = 0.3$	37%	14%	14%	6%	31%	2%	3%
GLF28 $\Delta T_e@\rho = 0.3$	9%	14%	12%	8%	24%	20%	16%
Weiland $\Delta T_i@\rho = 0.3$	Not Predicted	4%	43%	6%	14%	15%	2%
Weiland $\Delta T_e@\rho = 0.3$	Not Predicted	49%	12%	48%	1%	12%	2%

JG05.339-21c

Table 2 : Summary of the performances of the GLF23 and Weiland model for the shots of the dataset. The first line indicates the Greenwald fraction, second line the enhancement factor with respect to the IPB98 scaling (1). The lines below show the discrepancy on the prediction of ion and electron temperature at $\rho = 0.3$. Predictions within 20 % of the experimental value are highlighted in green, while red color indicate discrepancy larger than 20 % or strong disagreement in the profile slope between $0.3 < \rho < 0.8$.

	I_p (MA)	$n_{e0}/n_e^{(\rho = 0.95)}$	Q	β_N
DS03	13	1.0	10	2.65
DS03	13	1.5	13	3.0
GLF23	13	1.5	13	3.0
IPB98,high pedestal	13	1.5	4	1.8
IPB98, low pedestal	13	1.5	5	1.8

JG05.339-22c

Table 3 : Summary of the ITER projections performances for the different models and density peaking

I_p (MA)	$n_{e0}/n_e^{(\rho = 0.8)}$	Q	β_N	I_{NI}/I_p (%)	$I_{boot,\ ped}/I_p$ (%)	P_{LH} (MW)	Time of q = 1
11.3	1.0	4.9	2.2	45	11	0	490
11.3	1.0	4.7	2.5	68	15	20	925
13	1.5	13	3.0	59	17	0	650
13	1.5	11	3.5	77	25	20	1040

JG05.339-24c

Table 4 : Time of occurrence of the q *= 1 surface in ITER hybrid scenario for various plasma currents and LH power. Global confinement is given by the DS03 scaling.*

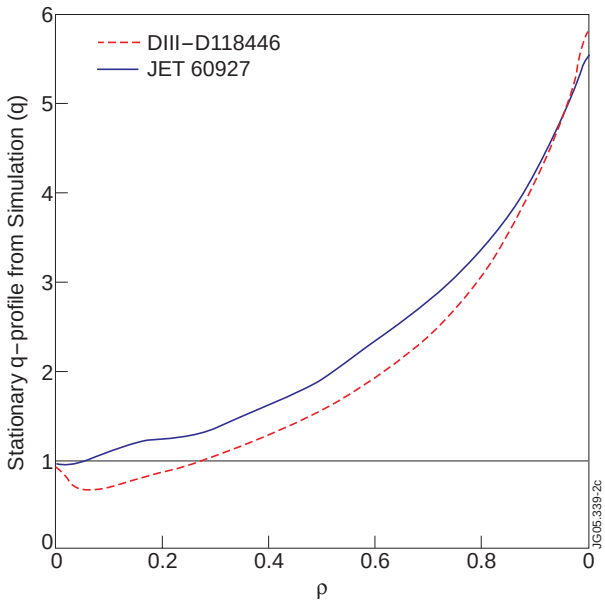

Figure 1: stationary q-profile solutions of the current diffusion simulations for shots DIIID118446 (dash red) and JET60927 (solid blue).

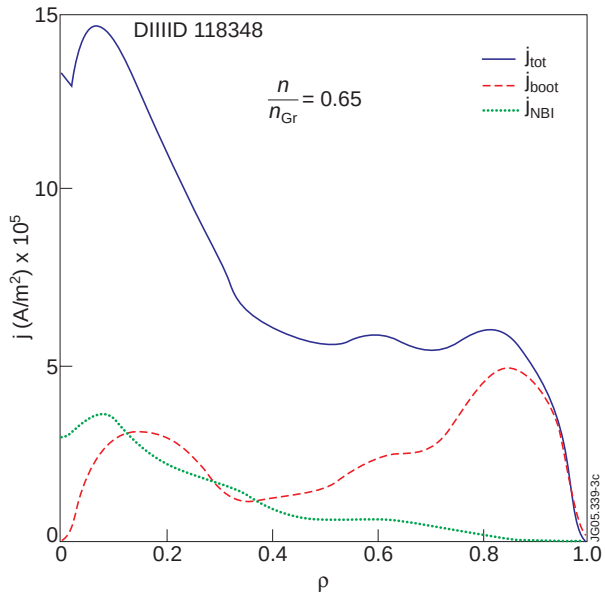

Figure 2: current density (solid blue) and non-inductive current drive (NBI in dash green, bootstrap in dash-dot red) profiles, for discharge DIII-D 118348.

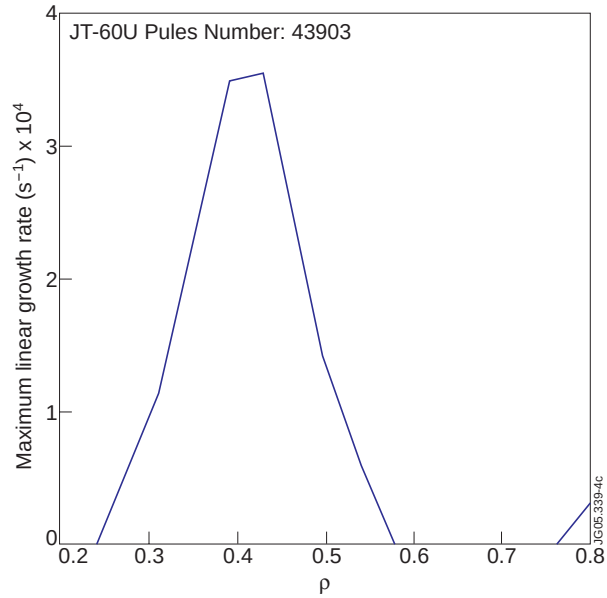

Figure 3: Profile of maximum linear growth rate calculated using KINEZERO for shot JT-60U 43903.

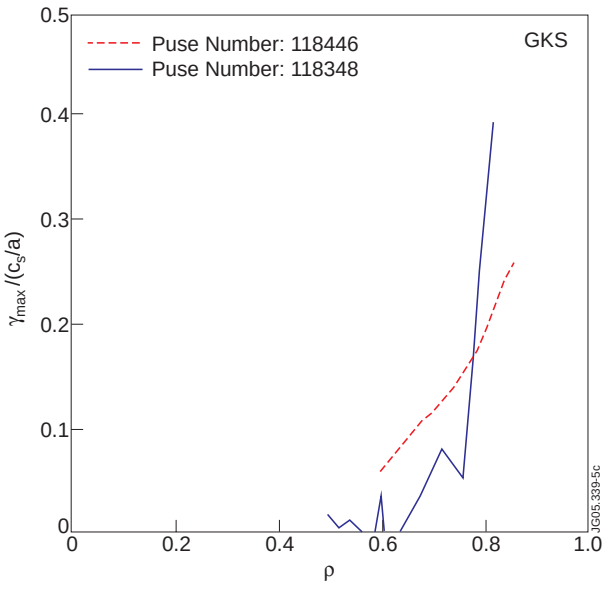

Figure 4: Profiles of maximum linear growth rate calculated using GKS for shots DIII-D 118446 (red) and DIII-D 118348 (blue).

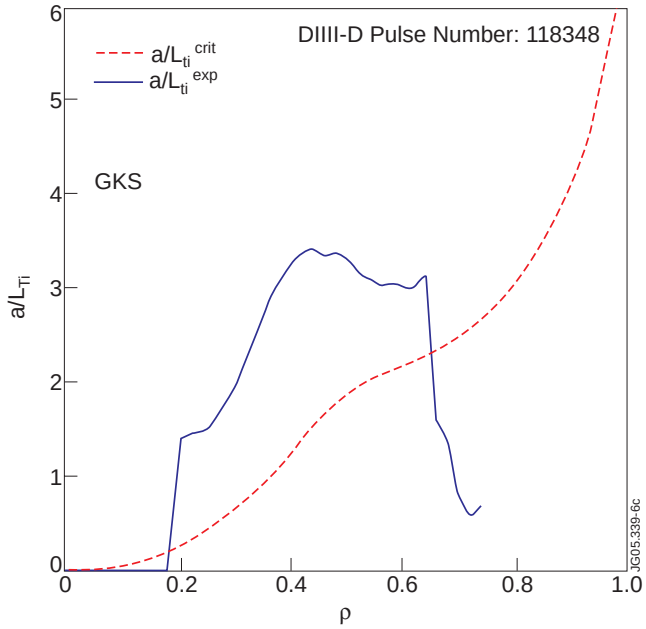

Figure 5 : Profiles of the critical threshold in a/L_{Ti} *(ion temperature) predicted by GKS (blue) and the experimental* a/L_{Ti} *(red), for DIII-D shot 118348.*

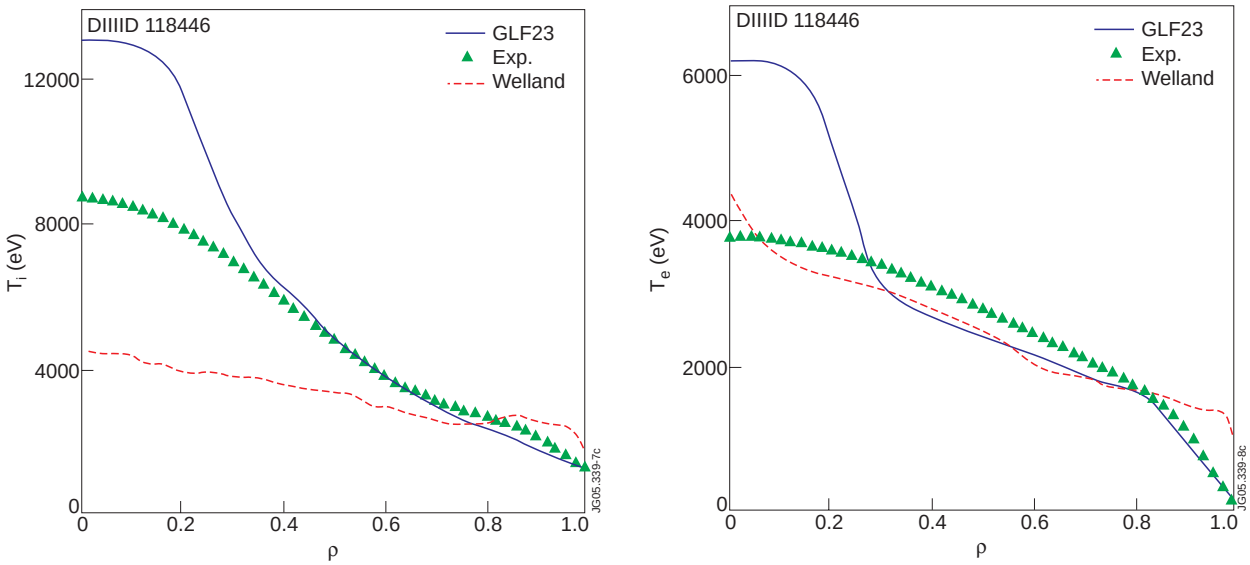

Figure 6 : T_i *(left) and* T_e *(right) profiles from the experiment (circles green), predicted by GLF23 (solid blue) and Weiland model (dash purple) for shot DIII-D118446 (*n/n_{Gr} *= 0.34)*

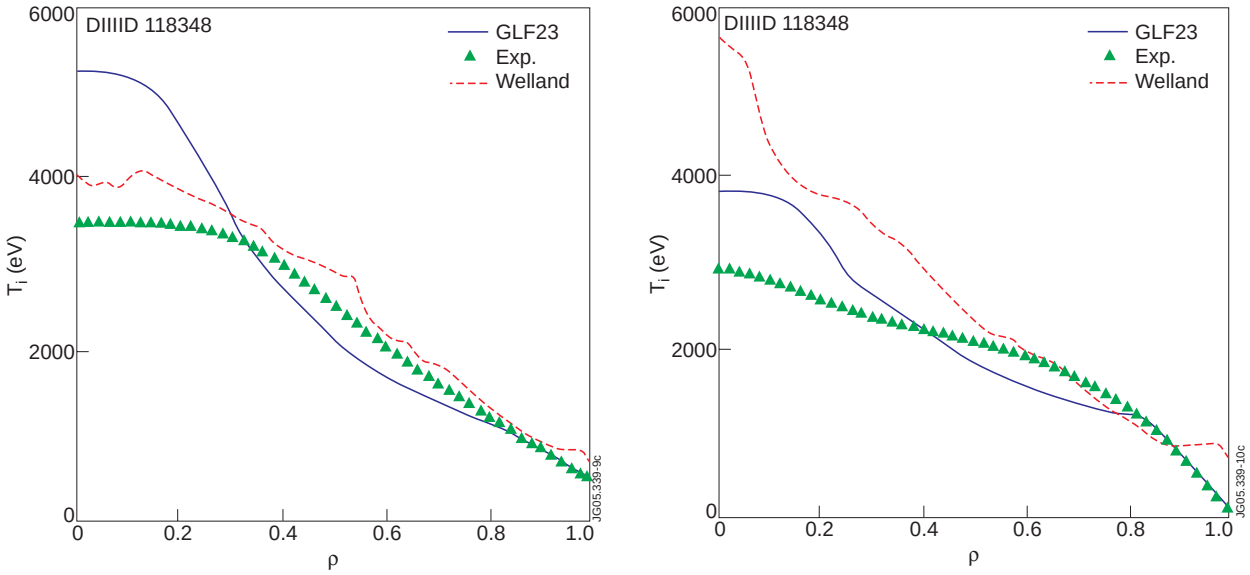

Figure 7 : T_i *(left) and* T_e *(right) profiles from the experiment (circles green), predicted by GLF23 (solid blue) and Weiland model (dash purple) for shot DIII-D118348 (*n/n_{Gr} *= 0.65)*

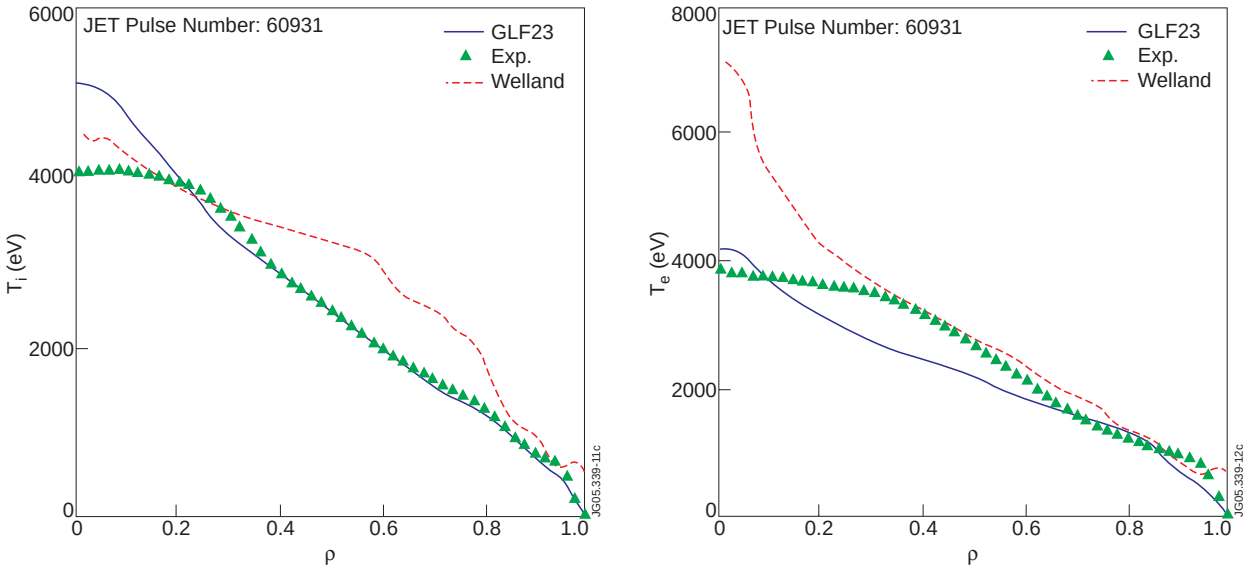

Figure 8 : T_i *(left) and* T_e *(right) profiles from the experiment (circles green), predicted by GLF23 (solid blue) and Weiland model (dash purple) for shot JET 60931 (*n/n_{Gr} *= 0.58)*

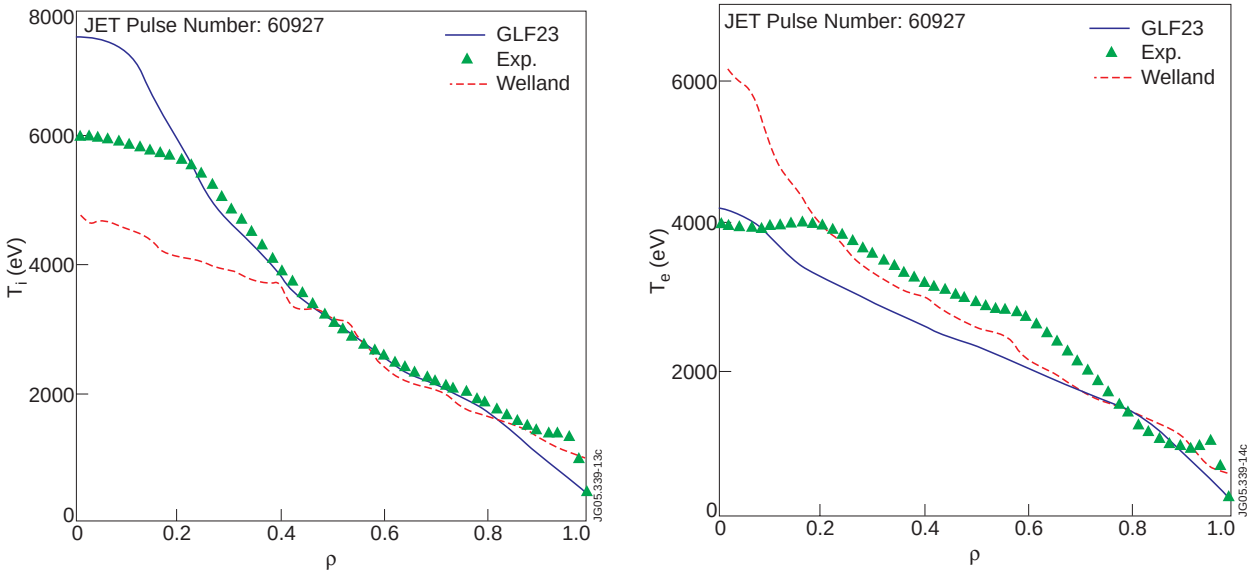

Figure 9: T_i *(left) and* T_e *(right) profiles from the experiment (circles green), predicted by GLF23 (solid blue) and Weiland model (dash purple) for shot JET 60927 (*n/n_{Gr} *= 0.61)*

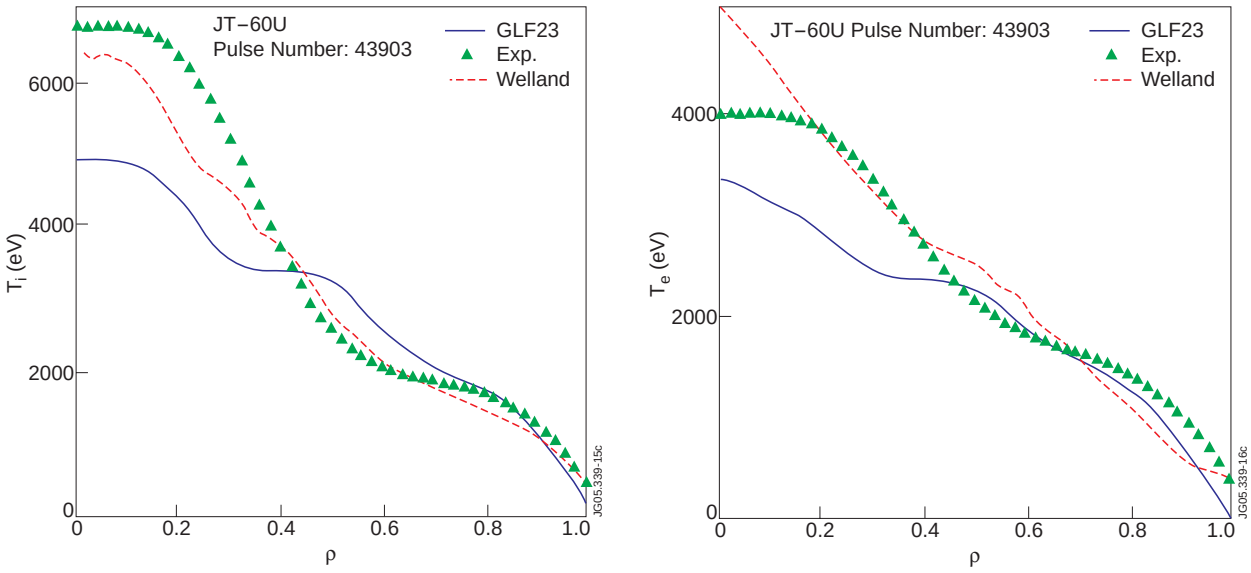

Figure 10: T_i *(left) and* T_e *(right) profiles from the experiment (circles green), predicted by GLF23 (solid blue) and Weiland model (dash purple) for shot JT-60U (*n/n_{Gr} *= 0.45)*

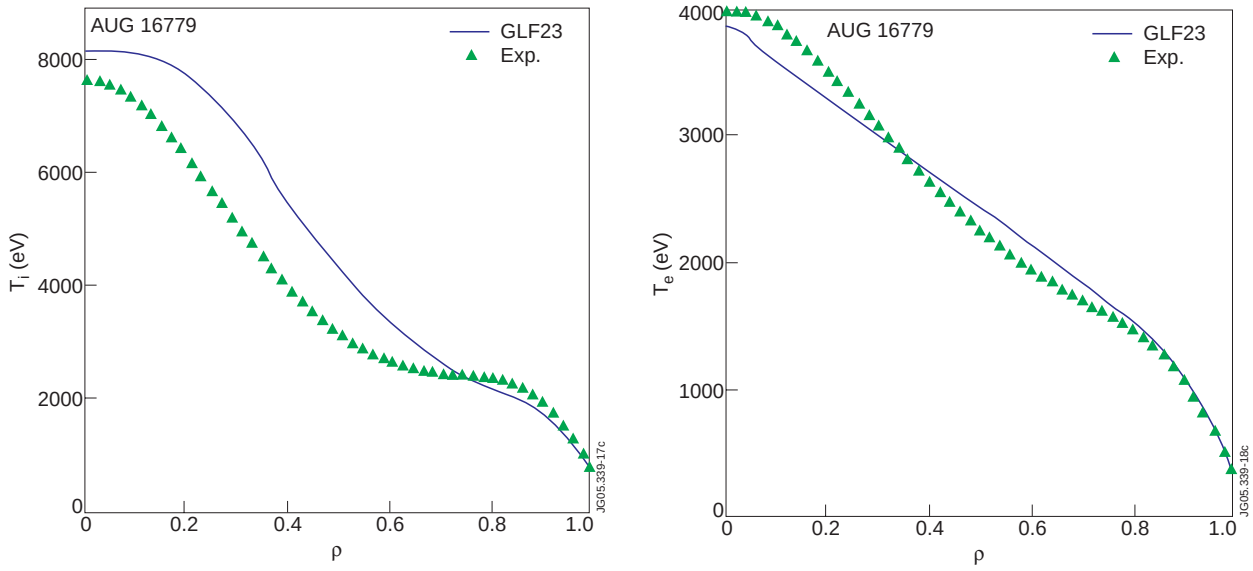

Figure 11: T_i *(left) and* T_e *(right) profiles from the experiment (circles green), and predicted by GLF23 (solid blue) for shot AUG 16779 (*n/n_{Gr} *= 0.34)*

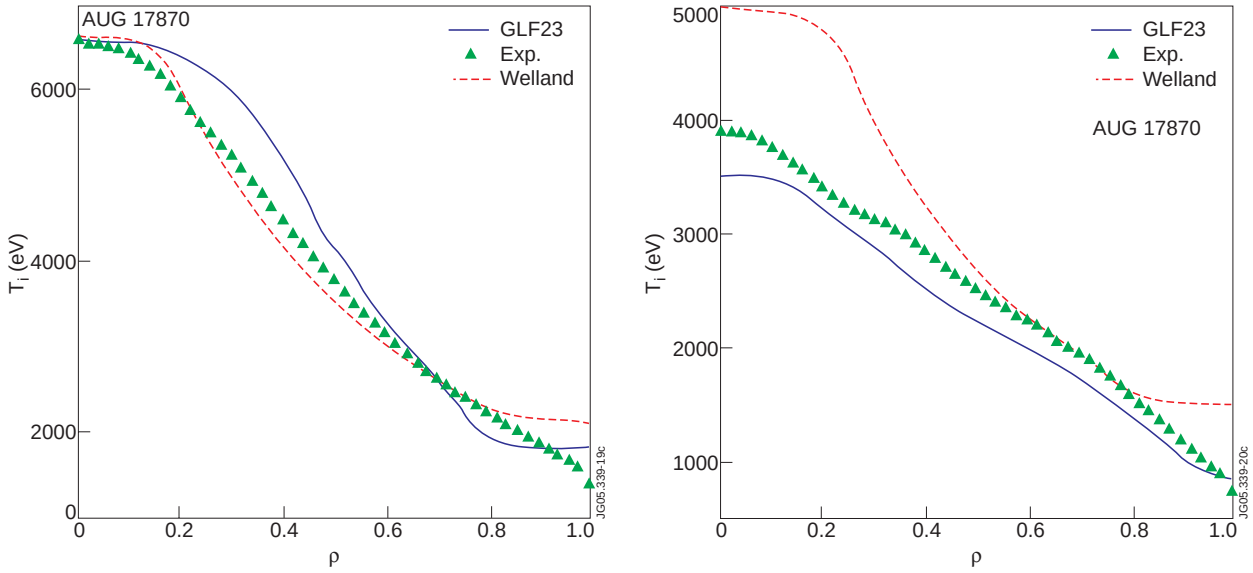

Figure 12: T_i *(left) and* T_e *(right) profiles from the experiment (circles green), predicted by GLF23 (solid blue) and Weiland model (dash purple) for shot AUG 17870 (*n/n_{Gr} *= 0.39)*

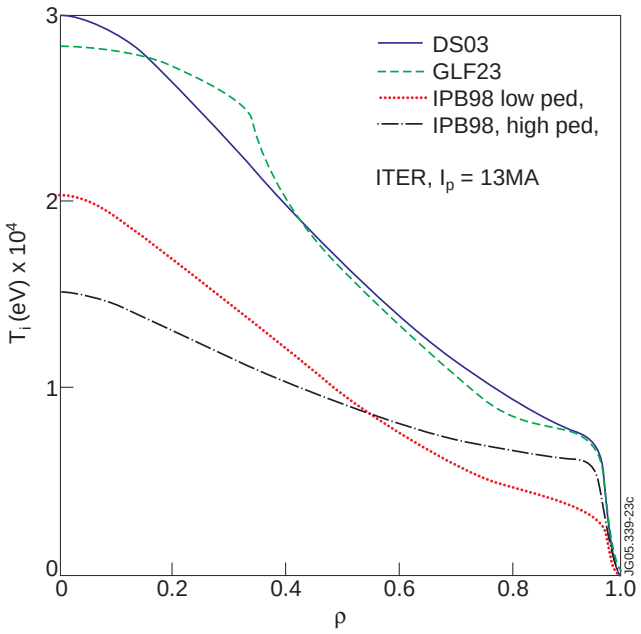

Figure 13: Ti profile obtained for the ITER projections corresponding to the bottom four lines of Table 3.

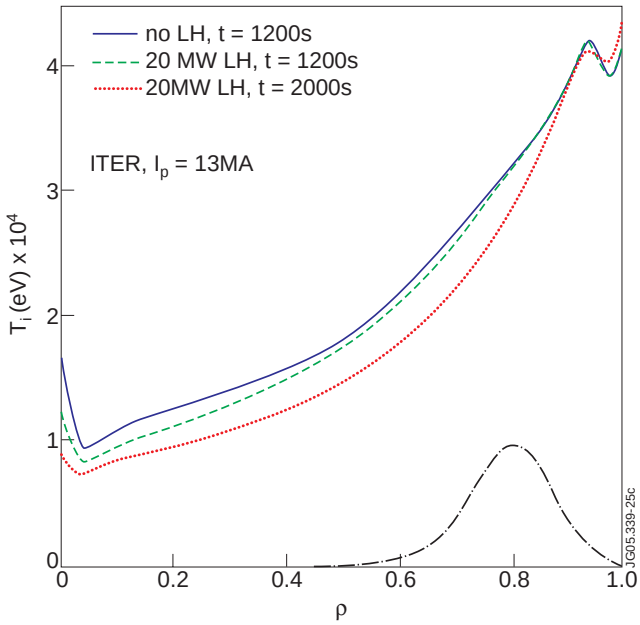

Figure 14: q*-profiles from various ITER hybrid scenario simulations at* I_p *= 13 MA, without LHCD at t = 1200 s (solid red), with 20 MW of LHCD at t = 1200 s (dash blue) and t = 2000 s (dash-dot green). The shape of the LH power deposition profile is indicated in arbitrary units (dash dot brown).*